Development of Current Controlled Grid-connected Microinverter for PV applications

Alaa Ismail, Mohamed Eldodor

University of Science and Technology at Zewail City, Egypt, s- alaaahmed@zewailcity.edu.eg, s-meldodor@zewailcity.edu.eg

Supervisor: Amgad Eldeib, Associate Professor, Renewable Energy Engineering Program Director
University of Science and Technology at Zewail city, Egypt, aeldeib@zewailcity.edu.eg

Abstract– Modern grid connected PV systems are becoming an integral part of zero net energy PV building integrated systems. Grid connected PV system topologies play a great role in harvesting the maximum available energy and determine the overall system efficiency. This work presents the development of a two-stage PV grid connected microinverter. The microinverter topology is based on using a low frequency transformer with a boost converter for the maximum power point tracking stage. The implementation phases included SIMULINK simulations and hardware development. Simulations of low frequency transformer-based topology achieved a system efficiency of 95 % with total harmonic distortion (THD) of 3%. The topology has proven an efficient tracking of the PV maximum power and DC link voltage set point. The hardware boards, DC-DC converter, DC-AC inverter, and control boards were all assembled and connected to the grid through a low-frequency transformer. The hardware achieved a conversion efficiency of the input energy of 94%.

Keywords—Microinverter, PV applications, two- stage DC/AC conversion.

I. INTRODUCTION

Photovoltaic (PV) energy is considered one of the most promising emerging technologies, thanks to its ever-increasing role in reducing carbon dioxide emissions [1]. The growth of the global PV market has been impressive since 2003, with an average annual growth rate of 40 % to 2009 and about 135% in 2010 [2]. Modern grid connected PV systems are becoming an integral part of buildings which are no longer considered energy consumers, but also energy producers. The European PV Industry Association (EPIA) states that with a total ground floor area of 22,000 km2, 40 % of the buildings roofs and 15% of the facades are suited for PV technology integration [2]. In sunny regions, global irradiance of at least 1200 kWh/m2/yr, PV integrated buildings can produce enough electricity for a family of two or three people for a year with an excess in spring and summer and a deficit in winter according to EPIA [2]. Consequently, the aim of reaching zero net energy buildings and even positive energy buildings is gaining a bigger interest. Hence, grid connected PV system topologies play a great role in harvesting the maximum available energy and determining the overall system efficiency.

Current topologies differ in terms of the used PV inverter which are categorized into central inverter, string inverter, DC optimizers with central inverter and microinverters. Microinverters are a module level topology, also named module integrated converted or AC module, mostly designed for power rating between 50 and 400 W with power conversion efficiencies above 90% [3]. Microinverter topologies are categorized into single stage and double stage microinverters. Single stage topologies boost the PV modules voltage to meet the grid requirements, track the maximum power and apply DC\AC conversion process within one stage, offering compact design and less components. While the double stage topologies boost the PV module voltage and track the maximum power in a separate stage besides applying the DC\AC conversion in another stage. Allocation of different functionalities in two independent stages simplify the control algorithm and adds a flexible input voltage range at the DC\DC converter [3].

Among the presented topologies, microinverters have gained a greater interest for PV systems due to their high capability of tracking the maximum power of each PV module separately despite the module orientation and shading conditions [4]. Since near-by structure shadings are regarded as the major challenge for energy harvesting of Building Integrated PV (BIPV) systems, microinverters can eliminate the effect of uneven incident radiation on the PV modules. Moreover, usage of microinverters eliminates the risk of arcs and firing by using only AC cables instead of DC cables [4]. However, selecting the microinverter topology has a great impact on the overall system efficiency. Furthermore, Egypt lacks microinverters suppliers and manufacturers, hence, the market need for this technology provides a great opportunity for offering this product. In the literature, the microinverter circuit was first modelled and implemented in the 1990s to have higher efficiency for solar energy conversion with a simple product that fits at the back of the solar panel [4][5][6]. The microinverter design can be either a single or double power stage. The double-stage microinverter differs from the single-stage ones in that it has a DC-DC conversion stage which is higher in efficiency and has a longer lifetime [7]. The microinverter discussed in [5][8][9] shows that coupling microinverter is either by using a high-frequency transformer positioned in the DC-DC converter, or by using a low-frequency transformer positioned before the grid. In the first case, a special converter, like a flyback converter, will be used to build up a DC link of more than 311 volts from 40-50 volts of the solar panel [8][9]. In the second case, an ordinary boost converter is implemented to build the DC link voltage to around 100 or 120 volts [8][9]. In this paper, we will start by implementing the most basic circuit of microinverters which is the low frequency microinverter. Section II presents the

6th IUGRC International Undergraduate Research Conference,
Military Technical College, Cairo, Egypt, Sep. 5th – Sep. 8th, 2022.

1

microinverter modelling and control. The hardware implementation is shown in section III. Results and discussion are presented in section IV.

II. MODELLING AND CONTROL

A. *Low frequency Microinverter Model*

The microinverter is implemented using a low frequency transformer. The low frequency transformer interfaces the inverter terminals with the grid and provides a means to step up the inverter voltage to the grid voltage (220 Vrms). Low frequency transformer is easier in development compared to the high frequency transformer, however; the size of low frequency transformer is bulky and so is its weight. In this section the modelling and control of the microinverter is described along with the topology operation mechanism to harvest the maximum power from PV panels and inject it to the grid. The microinverter includes two phases that play the role of tracking the PV maximum power and DC/AC conversion process. In this work, boost converter is implemented for the purpose of maximum power tracking using perturb and observe algorithm (P&O). The PV panel power, voltage and current ratings used in this work are 350, 43 V, 8 A respectively. The boost converter is sized to step up the PV panel voltage up to the DC link set point voltage, 150 V, then the current controlled voltage source converter performs the DC/AC conversion using a low frequency transformer. The selected control algorithm is the hysteresis control which adjusts the inverter current frequency and amplitude to the grid requirements. LCL filter is used at the interface of the VSC with the low frequency transformer to adjust the total harmonic distortion below 5% as stated by IEEE harmonics control requirements for systems rated from 120 V to 69 KV [10][11]. The simulation is performed using a 350 W solar panel with the irradiance and temperature of STC conditions 1000 W/m2 and 25 0C, respectively. Boost converter components sizing is based on the mentioned relations in [7], where the inductance design value is calculated from

$$Lmin = DR\ (1-D)^2/2f \quad (1)$$

However, the boost converter is not connected to a load but with the inverter keeping a constant voltage at the dc link capacitor, therefore Equation 1 is replaced with

$$Lmin = DVdc\ (1-D)^2/2fI \quad (2)$$

LCL filter sizing is selected by a trial-and-error approach due to the used current control method, Hysteresis control. In other words, the used control method is characterized by having unpredicted frequency value so that the filter design can be based on. The filter is designed such that the injected current waveform meets the THD specified by [11], switching frequency is below 90 kHz so that MOSFETS can be purchased easily.

B. *Low frequency microinverter Control*

Hysteresis current control is a method to control voltage source inverters where the actual current measured at the inverter terminals (I_{act}) is compared with the reference current
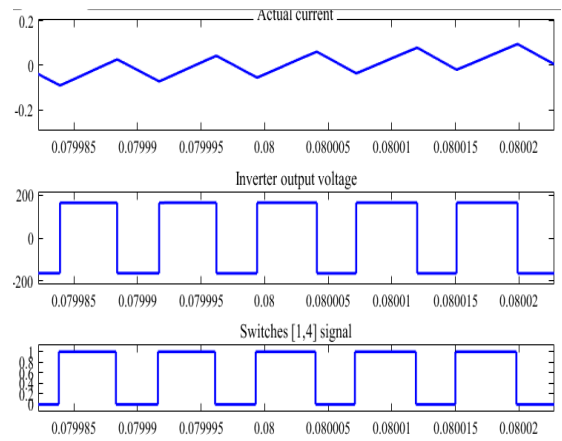

Fig. 1 Reference current and corresponding inverter voltage

of the grid (I_{ref}). The aim of this control method is to keep the actual current within a specified band higher and below the reference current so that the actual current tracks the grid current amplitude and frequency by means of switching. Comparison of the actual current with the higher and lower bands determine the pulse signal generated to maintain the inverter voltage level either at +Vdc or -Vdc. In other words, when the actual current exceeds the higher band the voltage level should be -Vdc by opening the switches (turning OFF) 1 and 4 while closing (turning ON) 2 and 3 and vice versa. The concept is shown in Fig. 1. The reference current is estimated using the DC link voltage, grid peak voltage and rated power of the inverter. DC link voltage is compared with a set point and the error is used as an input to a PI controller. Output of the PI controller is added to the power set point, the module's output power, and the result is divided by the DC link voltage; hence the current magnitude is obtained. Grid voltage waveform is divided by the peak voltage value to get a unity waveform with the grid operating frequency. The unity waveform is multiplied by the current magnitude to obtain the sinusoidal reference waveform that should be tracked. Actual current is measured and compared with the specified band [Iref - 0.05, Iref +0.05].

Selection of the current band affects the actual current total harmonic distortion (THD) where wide bands will have higher THD, then large LCL filter sizes will be required which increase the manufacturing size and cost. Narrow bands are preferred to get low THD however, higher switching frequency will be required to maintain the current within the bands which requires complex MOSFET sizing and increases the switching losses. Therefore, bands optimization while tracking the switching frequency is necessary for investigating the optimum design. After several simulation trials, the current band [difference between the higher and lower limit] is selected to be 0.1, the maximum switching frequency is estimated to be 90 kHz and the LCL filter size selected is 6 mH, 10 nF and 2 mH, respectively.

III. HARDWARE IMPLEMENTATION

According to the simulations of the microinverter the hardware was divided into three main parts: DC-DC Boost Converter,

6th IUGRC International Undergraduate Research Conference,
Military Technical College, Cairo, Egypt, Sep. 5th – Sep. 8th, 2022.

DC/AC single phase inverter, control, and Power supply. Each part will be designed and manufactured in the following sections.

A. DC-DC boost converter

Based on the simulation, the boost converter main parts needed for having the control and performance like the software, are the power switching devices as the MOSFET and the Diode, the filtering components as the input inductor and the output capacitor, and the measurement components required as the input current and voltage and the output voltage sensors.

1. Power components design

Starting with the power components, the simulation provides us with ratings needed for each component. The ratings needed for designing the MOSFT are V_{max} of 164 V, V_{rms} of 82 V, I_{max} of 8.7 A, and I_{rms} of 7.2 A. IRFP260N MOSFET is chosen as a suitable candidate, and by using its datasheet its losses are calculated to be found 1.5 W for conduction losses and 6.2 W for the switching losses, so the total losses are 7.7 W.

The second power component is the diode. The ratings needed for designing the diode are V_{max} of 159 V, V_{rms} of 135 V, I_{max} of 8.2 A, and I_{rms} of 4.1 A. The selection of the diode depends mostly on satisfying its voltage and current ratings and having the lowest forward voltage to have low diode losses. By satisfying these two conditions and calculating the losses to be found at 3.18 Watts, the choice was for BYW29-200 diodes.

2. Filter components design

The input inductor needed characteristics are a maximum current of 8.25A and an inductor value of 3mH. Based on the max current flowing in the wire turns of the inductor, the wire diameter was determined and chosen based on the AWG. A wire of 1mm diameter was selected. Also, an air gap was done to stop the saturation of the toroid core and make sure that the current will flow up to 10A. The design was implemented and tested already on a working boost converter. By having a 5 m wire length and resistance/length value of 21 milliohm/meter, the total resistance of the inductor equals around 0.1 ohms, which resulted in a total loss in the inductor of around 4.5W at the converter-rated operation.

3. Measurement sensors

The measurement of the input and output voltages was implemented by using a simple voltage divider, that can reduce the 40 V or 150 V of the input and output voltages respectively, to less than 5 volts that the microcontroller can tolerate. A small filtering capacitor of 1 or 10 microfarads was used to smooth the measured voltages. The measurement of the input current was done by using a series resistor. The idea of this sensor is to use an extremely low series resistance with the solar panel, to make a low voltage drop on it, to have an extremely low losses in it, and by using operational amplifier circuit this signal can be amplified to significant values that the microcontroller can tolerate. The schematic of this sensor circuit is shown in Fig. 2.

The boost converter hardware PCB schematic and hardware are shown in Fig. 3 and Fig. 4, respectively, with each component illustrated in Table 1.
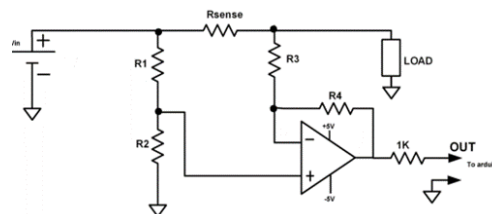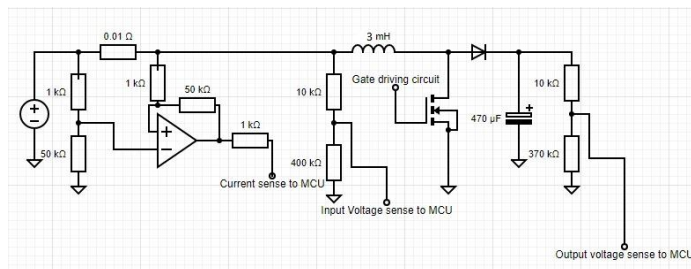

Fig. 2 Current measurement for DC-DC Converter

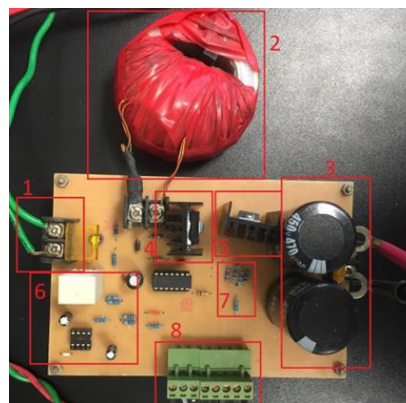*Fig. 3 DC-DC converter circuit schematic*

Fig. 4 DC-DC converter board

Table 1 DC DC converter board items

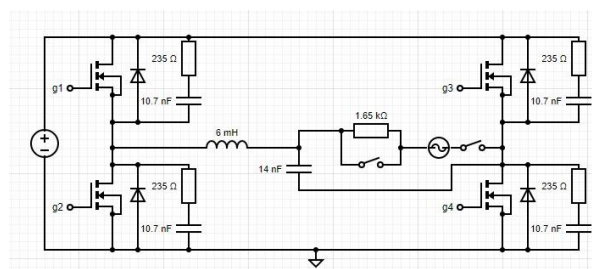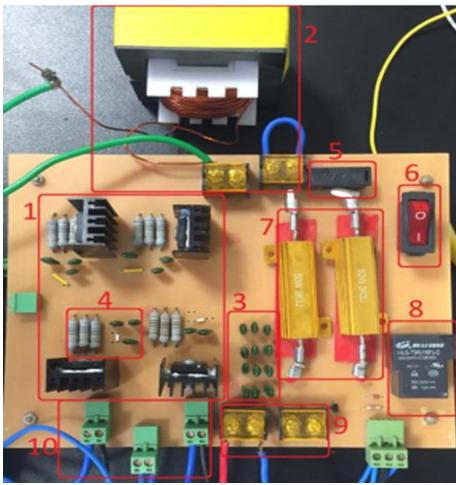|	
1	Solar Panel input.
2	Boost converter inductor.
3	DC-link Capacitor.
4	Boost converter MOSFET.
5	Boost converter Diode.
6	Input current sensor.
7	Output voltage sensor.
8	Voltages and signals from and to the control board.

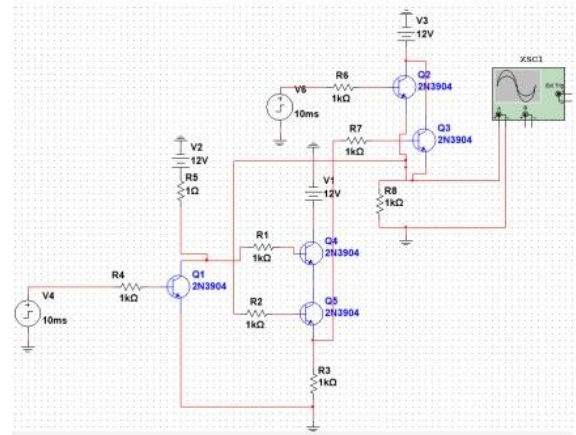*Fig. 5 DC-AC inverter circuit schematic*

Fig. 6 DC-AC inverter board

Table 2 DC/AC inverter board items

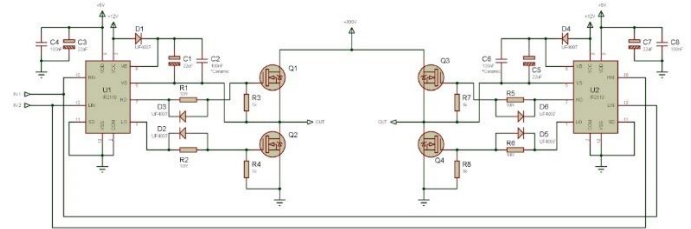|	
1	Single phase MOSFET bridge.
2	Filter Inductor.
3	Filter Capacitor.
4	Snubber Circuit.
5	Fuse.
6	ON/OFF switch
7	Series Resistance (for the soft starting).
8	Parallel relay to the series resistance.
9	Grid input.
10	Input pulses from the control board.

B. DC-AC single phase inverter

The power device of the inverter is the most vital component that needs to be designed precisely to avoid burning it. The simulation provides us with ratings needed for designing the MOSFET which are: V_{max} of 164 V, V_{rms} of 82 V, I_{max} of 7 A, and I_{rms} of 4.5 A. From the Max Voltage, it is decided that a MOSFET with a drain to source voltage of at least 250V is needed. Also, IRFP260N is a good MOSFET, however if it is used, it would be needed to design a snubber circuit to smooth the on and off switching of the MOSFET. Also, I need it to have the lowest rise and fall time to decrease the switching losses, as with the control scheme used there is no control on the switching frequency, which leads to having a range of switching frequencies during the operation. The inverter hardware schematic and PCB design are shown in Fig. 5 and Fig. 6, respectively, with each component illustrated in Table 2.
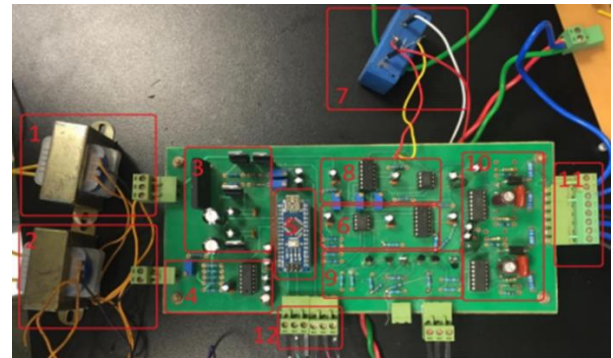

Fig. 7 Control circuit schematic

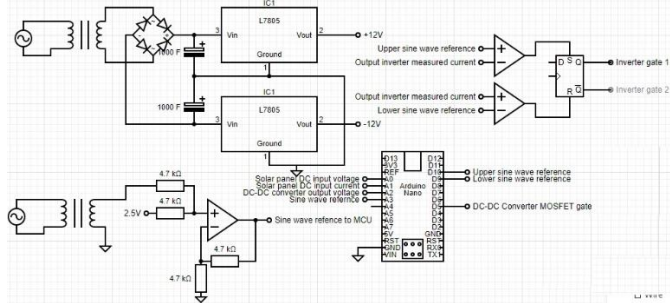**6th IUGRC International Undergraduate Research Conference,**
Military Technical College, Cairo, Egypt, Sep. 5th – Sep. 8th, 2022.

4

Fig. 8 SR flip flop circuit schematic

Fig. 9 Inverter's MOSFETS gate drivers

Fig. 10 Control and power supply board

C. Control and Power supply

Based on the simulation, the control main parts needed for having the control and performance as implemented in the software is shown in Figures 7,8,9,10 and illustrated in Table 3.

IV. RESULTS AND DISCUSSION

A. Simulation Results

Simulations of the low frequency converter topology are developed using PV module, with specification presented in Table 4, at irradiance and ambient temperature of 1000 W/m2 and 25 ^{0}C respectively. MPPT results are shown in Fig. 11, where the PV output power is 349 W. MPPT adjusts the duty to be 0.7 to satisfy the DC link voltage and *Vmpp* ratio. Fig. 12 represents the microinverter injected power to the grid (333 W). The considered losses are boost converter inductor losses, boost converter switching and conduction losses, LCL filter losses and low frequency transformer winding losses. Topology efficiency is estimated to be 95.4 %.

Table 3 Control and power board items

1	Power supply transformer.
2	Reference sine wave transformer
3	Rectifier power supply circuit (generates 12V, -12V, 5V, 1V & 2.5V)
4	Sine wave summing amplifier for the reference sine wave to the Arduino.
5	Arduino Nano Microcontroller.
6	Reference sine wave DAC and amplifier circuits
7	Actual current measurement sensor.
8	Comparator circuit between the actual and the reference currents.
9	Flip-Flop circuit
10	Inverter's MOSFETs gate driver circuit.
11	Output to the inverter board.
12	Output to the converter board.

Table 4 PV module specifications

Parameter	Value
Maximum power (Pmpp)	350 W
Maximum power point current (Impp)	8.13 A
Maximum power point voltage (Vmpp)	43 V
Open circuit voltage (Voc)	51.5 V
Short circuit current (Isc)	9.4 A
Temperature coefficient of Voc	-0.36 % / ^{0}C
Temperature coefficient of Isc	0.09 % / ^{0}C

Table 5 Microinverter parameters

Parameter	Value
Boost converter inductance	5e-4 H
Inductor resistance	0.01 Ω
MOSFET Ron	0.04 Ω
DC link capacitance	1 mF
LCL filter	6 mH – 10 nF – 2mH
Transformer turns ratio	1:3
Primary coil resistance	0.2 Ω
Secondary coil resistance	1.2 Ω
Primary coil inductance	43 mH
Secondary coil inductance	0.35 H
DC link voltage set point	150 V

DC link voltage waveform is represented in Fig. 13, showing the voltage oscillations around voltage set point ,150 V, which guarantees that the total DC/DC converter is injected to the inverter, i.e., Zero average capacitor current. Peak to peak voltage ripples is estimated to be 8 V, 5% of the voltage set point, based on the selected value of DC link capacitance, 1mF.

Current waveforms are represented in Fig. 14, showing maximum current value 6 A and RMS value of 4.6 A. The waveforms satisfy the grid requirement frequency and THD where the estimated values are 50 Hz and 3%, respectively.

B. Experimental Results

After making sure that the converter and the inverter boards are working properly, the next step is to connect the power supply to the inverter through the DC-DC converter where the converter task is to maintain the DC link voltage constant at 150

V. and the inverter is connected to the grid through a 94/220 Volts 50Hz transformer. In this test, the current reference of the inverter is set as a constant value. The hardware setup is shown as follows in Fig. 16.
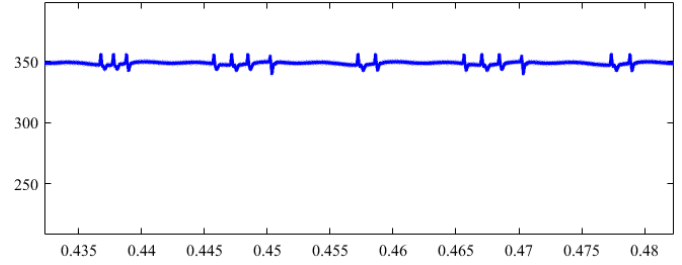

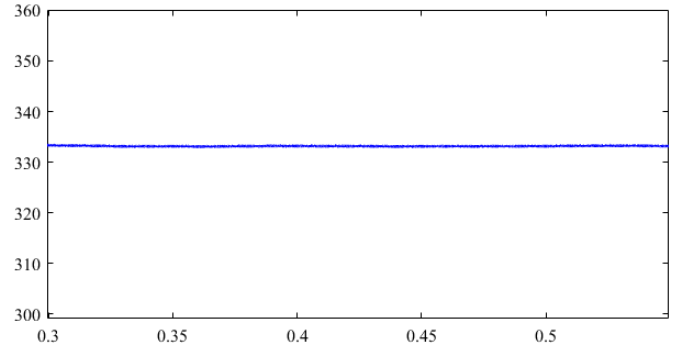Fig. 11 PV module output power

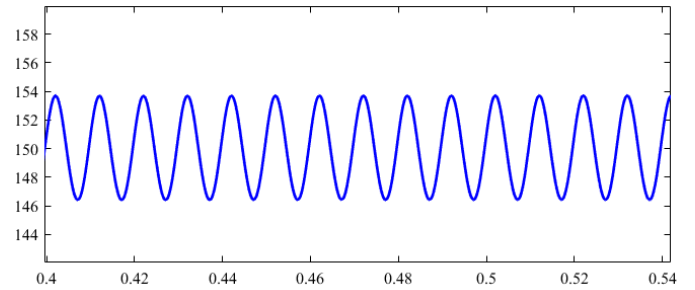
Fig. 12 Microinverter output power

Fig. 13 DC link voltage
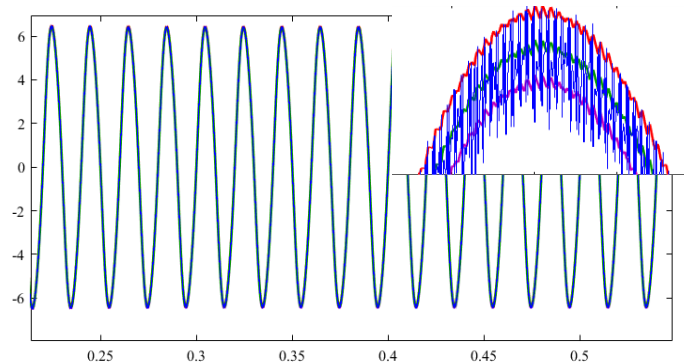
Fig. 14 Microinverter current and bands

6th IUGRC International Undergraduate Research Conference, Military Technical College, Cairo, Egypt, Sep. 5th – Sep. 8th, 2022.

5

Fig. 15 Current total harmonic distortion

Fig. 18 Result for 3 amperes refence current
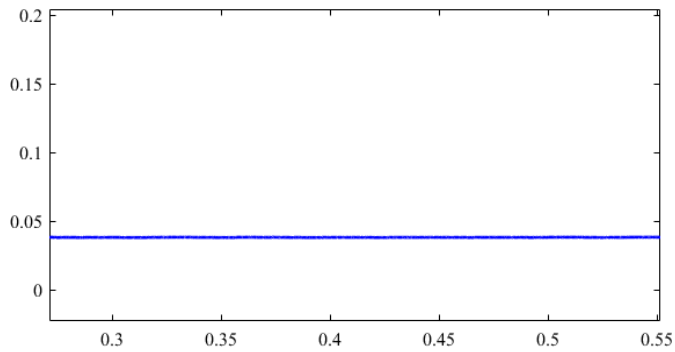
The results of this trial with the reference current set to peak value of 2 amperes and 3 amperes, is given as in Fig. 17 and 18, respectively, where the actual current and the set current compared to each other. The goal now is to apply the same control loop implemented in Simulink earlier, where the DC-DC converter task is to apply the maximum power point tracking, and the inverter task is to fix the DC link voltage to 150 V.

The only problem in the DC-DC converter while using an ordinary power supply at its input, not a PV panel, is that whatever the change in the duty cycle, the input voltage will not change, and hence the input power will not change, and this leads to no current being injected into the grid. That is why to emulate the solar panel performance a series and shunt resistors are fixed between the DC-DC converter and the power supply.
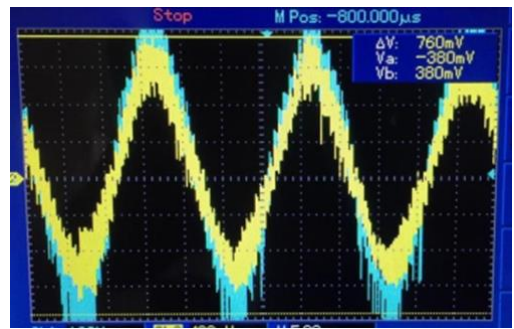
The series resistor value is 3.3 ohms, and the parallel resistor is 470 ohms. The performance of the input voltage curve to the converter is shown in Figures 19 and 20. The hardware setup for the whole inverter working the power supply that is emulating the solar panel is shown in Fig. 21.
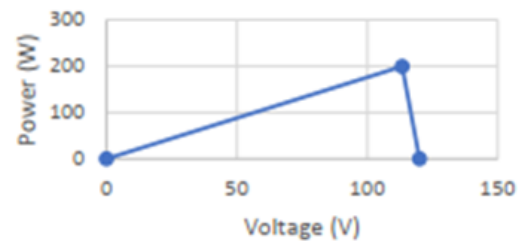

Fig. 19 Input source, Power vs Voltage characteristics
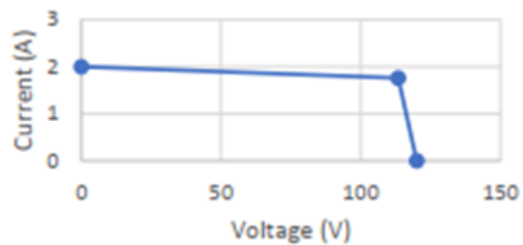

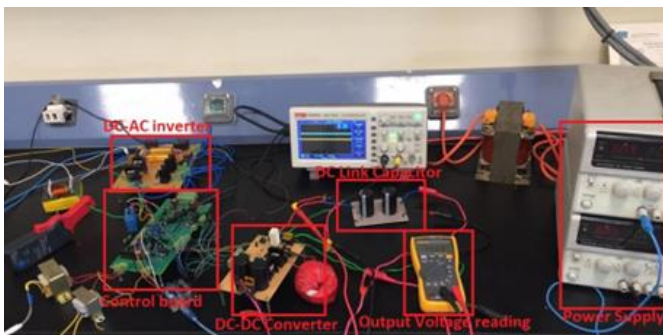Fig. 20 Input source, Current vs Voltage characteristics

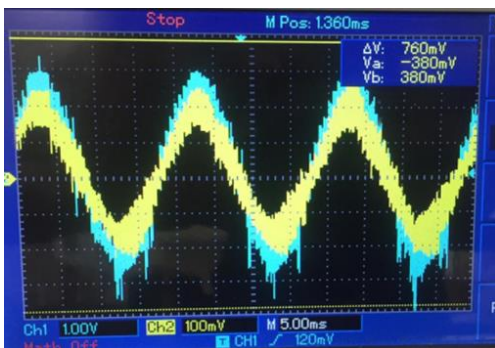Fig. 16 Hardware setup for inverter operation with constant reference current

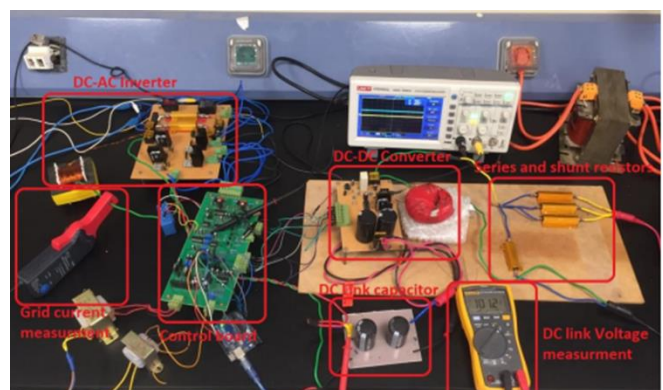Fig. 17 Result for 2 amperes refence current

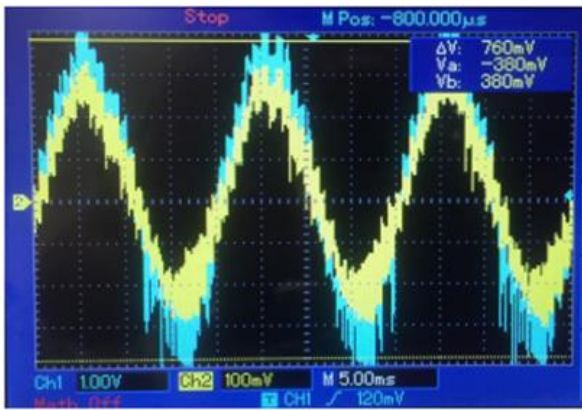Fig. 21 Hardware setup for inverter operation with full control functions.

6th IUGRC International Undergraduate Research Conference, Military Technical College, Cairo, Egypt, Sep. 5th – Sep. 8th, 2022.

Fig. 22 Injected current for the inverter operation with full control functions.

The maximum power point was achieved and based on it a refence current of 2.12 Amperes was injected to the grid, while the DC link voltage was kept constant at 150V. The output real power of the inverter was 172.69 Watts, while the input power to the converter after the series and parallel resistors was 182.4. The current waveform of this operation is shown in Fig. 22.

V. CONCLUSION

This work presented a microinverter, which converts DC power from a solar panel to supply AC grid power. A literature review and methodology sections have been carried out to select a suitable topology for the inverter. The two-stage microinverter is chosen with a DC/DC boost converter and DC/AC converter coupled with the grid through a transformer, for prototyping the low frequency method. The movement towards the Microinverter was in order to increase the total efficiency of the solar sites and have full control in each panel without disturbing the other panels. The low frequency transformer based Microinverter topology was implemented to test the control and the operation of connection to the grid. The DC-DC converter stage was implemented and was proven to achieve the maximum power point tracking using the setup of an input power supply and an output resistance. The DC-AC inverter along with the control was implemented and proven to achieve the current set point targeted and being in phase with the reference current using the setup of input power supply and output connected to the grid through a transformer.

The disadvantages of low frequency transformer lie in the large size and high losses, therefore topologies with high frequency transformer qualifies will be used as a future work to investigate the microinverter operation with it. Topologies that include high frequency transformer of interest are the two-switch flyback and boost flyback. These topologies will be compared in terms of efficiency, size and hardware implementation.

REFERENCES

[1] Hasan, R., Mekhilef, S., Seyedmahmoudian, M. and Horan, B., 2017. Grid-connected isolated PV microinverters: A review. *Renewable and Sustainable Energy Reviews*, 67, pp.1065-1080.

[2] International Energy Agency (IEA). Solar energy prespectives, 2011. Available at: https://webstore.iea.org/download/direct/558?fileName=Solar _Energy_Perspectives2011.pdf.

[3] Çelik, Ö., Teke, A. and Tan, A., 2018. Overview of micro-inverters as a challenging technology in photovoltaic applications. *Renewable and Sustainable Energy Reviews*, 82, pp.3191-3206.

[4] Rezaei, M., Lee, K. and Huang, A., 2016. A High-Efficiency Flyback Micro-inverter With a New Adaptive Snubber for Photovoltaic Applications. *IEEE Transactions on Power Electronics*, 31(1), pp.318-327.

[5] Y. Xue, L. Chang, and S. B. Kjær, "Topologies of SinglePhase Inverters for Small Distributed Power Generators: An Overview," IEEE Tran. on Power Electronics, vol. 19, no. 5, pp. 1305–1314, 2004.

[6] Q. Li and P. Wolfs, "A Review of the Single Phase Photovoltaic Module Integrated Converter Topologies With Three Different DC Link Configurations," IEEE Tran. on Power Electronics, vol. 23, no. 3, pp. 1320–1333, 2008.

[7] A. C. Kyritsis, E. C. Tatakis, and N. P. Papanikolaou, "Optimum Design of the Current-Source Flyback Inverter for Decentralized Grid-Connected Photovoltaic Systems," IEEE Tran. on Energy Conversion, vol. 23, no. 1, pp. 281– 293, 2008.

[8] S. B. Kjaer, J. K. Pedersen, and F. Blaabjerg, "A Review of Single-Phase Grid-Connected Inverters for Photovoltaic Modules," IEEE Trans. on Industry Applications, vol. 41, no. 5, pp. 1292–1306, 2005.

[9] S. Park, G. Cha, Y. Jung, and C. Won, "Design and Application for PV Generation System Using a SoftSwitching Boost Converter With SARC," IEEE Trans. on Industrial Electronics, vol. 57, no. 2, pp. 515–522, 2010.

[10] H.-W. Seong, H.-S. Kim, K. Park, G.-W. Moon, and M.-J. Youn, "High Step-Up DC-DC Converters Using ZeroVoltage Switching Boost Integration Technique and LightLoad Frequency Modulation Control," IEEE Tran. on Power Electronics, vol. 27, no. 3, pp. 1383–1400, 2012.

[11] "IEEE Recommended Practices and Requirements for Harmonic Control in Electrical Power Systems." doi:10.1109/ieeestd.1993.114370.

6ᵗʰ IUGRC International Undergraduate Research Conference, Military Technical College, Cairo, Egypt, Sep. 5ᵗʰ – Sep. 8ᵗʰ, 2022.